sustainability

MDPI

Article

Wheat-Straw-Derived Activated Biochar as a Renewable Support of Ni-CeO_2 Catalysts for CO_2 Methanation

Christian Di Stasi [1,*], Simona Renda [2], Gianluca Greco [1], Belén González [1], Vincenzo Palma [2] and Joan J. Manyà [1]

[1] Aragón Institute of Engineering Research (I3A), Thermochemical Processes Group, Escuela Politécnica Superior-University of Zaragoza, Crta. Cuarte s/n, 22071 Huesca, Spain; greco@unizar.es (G.G.); belenglez@unizar.es (B.G.); joanjoma@unizar.es (J.J.M.)

[2] Department of Industrial Engineering, University of Salerno, Via Giovanni Paolo II 132, 84084 Fisciano, SA, Italy; srenda@unisa.it (S.R.); vpalma@unisa.it (V.P.)

* Correspondence: christiandistasi@unizar.es

Abstract: Ceria- and urea-doped activated biochars were used as support for Ni-based catalysts for CO_2 methanation purposes. Different materials were prepared and tested to find the best catalytic formulation. After several CO_2 methanation experiments—carried out at 0.35–1.0 MPa and 300–500 °C—it was found that the most suitable catalyst was a wheat-straw-derived activated biochar loaded with 30 wt.% of CeO_2 and 20 wt.% of Ni. Using this catalyst, a CO_2 conversion of 65% with a CH_4 selectivity of 95% was reached at 1.0 MPa, 400 °C, and 13,200 h^{-1}. From the study of the influence of the gas hourly space velocity, it was deduced that the most likely reaction mechanism was a reverse water–gas shift reaction, followed by CO hydrogenation. N-doping of the carbon support as an alternative to the use of ceria was also investigated. However, both CO_2 conversion and selectivity toward CH_4 values were clearly lower than those obtained for the ceria-containing catalyst cited above. The outcomes of this work indicate that a renewable biomass-derived support can be effectively employed in the catalytic conversion of CO_2 to methane.

Keywords: CO_2 methanation; Sabatier reaction; biochar; urea; ceria

Citation: Di Stasi, C.; Renda, S.; Greco, G.; González, B.; Palma, V.; Manyà, J.J. Wheat-Straw-Derived Activated Biochar as a Renewable Support of Ni-CeO_2 Catalysts for CO_2 Methanation. *Sustainability* **2021**, *13*, 8939. https://doi.org/10.3390/su13168939

Academic Editors: Matthew Jones and Changhyun Roh

Received: 30 June 2021
Accepted: 6 August 2021
Published: 10 August 2021

1. Introduction

Since the second industrial revolution, human civilization started to be highly dependent on fossil fuels. Their continuous exploitation resulted in the increase in the atmospheric CO_2 content, which is associated with several environmental issues [1–3]. In recent years, different strategies have been postulated to substantially reduce CO_2 emissions. Among them, coupling carbon capture utilization (CCU) with power-to-gas (PtG) schemes could represent a very promising option [4,5]. Through this approach, the electric energy produced from renewable sources is used to produce hydrogen via water electrolysis. The resulting hydrogen and the CO_2 sequestered from power plants or industrial processes are then employed as reactants for the Sabatier reaction (Equation (1)) to produce methane, which—unlike hydrogen—could easily be injected into the national grid.

$$CO_2 + 4\,H_2 \rightleftharpoons CH_4 + 2\,H_2O;\ \Delta H_{298K} = -165\ \text{KJ mol}^{-1} \quad (1)$$

The reaction is highly exothermic and generally carried out in the temperature range of 200−500 °C. However, CO_2 conversion toward CH_4 involves high activation energies, which make the reaction less likely at relatively low temperatures [6]. Therefore, the use of an appropriate catalyst is mandatory. Noble metals-based catalysts—such as Ru [7], Rh [8], and Pt [9]—have been reported to be active and selective for methanation purposes. However, their high cost and limited availability encouraged research into cheaper alternatives, such as transition metal-based catalysts. Among the latter, Ni-based catalysts appear as a

promising option due to their low cost and remarkable catalytic performance [10–12]. Since the main role of nickel is to dissociate H_2 molecules [13], a catalyst support that is able to adsorb and activate a large amount of CO_2 is essential for a successful catalytic formulation. To this end, reducible metal oxides, such as ZrO_2 [14] and CeO_2 [15], have been extensively used due to the presence of surface oxygen vacancies at the interface between the active metal and support. In the case of Ni/Ceria catalyst, Renda et al. [9] obtained outstanding performances in terms of methane yield (75%) and CO_2 conversion (73%) at 0.1 MPa and 350 °C. Meanwhile, Alarcón et al. [16] achieved, with an $Ni/CeO_2/\gamma\text{-}Al_2O_3$, a stable CO_2 conversion of 90% for at least 120 h.

Carbon-based supports like activated carbon and carbon nanotubes [17–22] are gaining attention because of their chemical stability and surface chemistry tunability. However, the main problem related to these materials is that their production is usually highly energy consuming. Another drawback is that their highly microporous structure could result in diffusional limitations of both reactants and products. Moreover, in the absence of certain surface functional groups, the interaction between the metallic active phase and the support is poor, leading to metal sintering phenomena [20]. To improve the properties of carbonaceous supports, the introduction of N-containing functional groups appears as a very promising approach. In addition to the enhanced electronic interaction, nitrogen doping could also lead to the incorporation of basic sites within the carbon framework, resulting in an enhanced CO_2 adsorption [23,24].

From a sustainability point of view, renewable carbon materials are excellent candidates to be used as catalyst supports. For instance, biochar—an aromatic carbon-rich solid produced via slow pyrolysis of biomass [25]—is currently receiving growing interest as a potential starting material for advanced catalytic applications, owing to its low cost and versatility [26]. The addition of this biomass-derived material to the most effective catalytic formulations (e.g., Ni/Ceria) could notably decrease the overall catalyst cost; also, at its end-life stage, the carbon support could be burnt to recover energy and active phases [27]. However, there are still very few studies in literature describing the performance of biochar-based metal catalysts in CO_2 methanation. Among them, Wang and co-workers produced and tested Ni- and Ru-based catalysts supported on ceria- [28] and urea-doped biochar [23]. Their results showed very good CO_2 conversion, even at low temperatures. Nevertheless, ceria and urea were added to the raw biomass, instead of biochar. To strengthen the value chain of biochar systems, it seems more interesting to produce engineered biochar-derived materials as value-added products, which can generate important revenues for large-scale biochar production systems.

In this work, a wheat-straw-derived activated biochar was produced and then doped with CeO_2 to produce Ni-based catalysts, which were then tested for CO_2 methanation. Several catalytic experiments were carried out at different temperatures, pressures, and gas space velocities to find the optimal catalytic formulation and operating conditions. Furthermore, urea-doped activated biochars were also synthesized and used as catalyst supports to assess the influence of the surface N-containing functional groups on the catalytic performance.

2. Materials and Methods

2.1. Materials

Wheat straw pellets were pyrolyzed under N_2 atmosphere at 500 °C and atmospheric pressure. Details concerning the pyrolysis device and procedure can be found in a previous article [29]. The resulting raw biochar was crushed and sieved to obtain particle sizes within the range of 0.212–1.41 mm. Then, biochar was physically activated with CO_2 at 700 °C and 1.0 MPa for 2 h in a fixed-bed reactor (made of alloy UNS N06600, 28.1 mm ID, and 600 mm long). These operating conditions were proven to be effective to obtain a material with a more hierarchical pore size distribution [30].

The catalysts tested in this work were prepared via wet impregnation of the above-mentioned activated biochar using $Ce(NO_3)_3{\cdot}6H_2O$ or $CO(NH_2)_2$ (urea) as dopant agents.

The aqueous solutions were stirred at 80 °C until complete water evaporation and then dried overnight at 110 °C. The resulting dried mixtures were finally calcined at 550 °C for 3 h under inert atmosphere (N_2) using the above-mentioned reactor. The doped activated biochars were then impregnated with an aqueous solution of $Ni(NO_3)_2 \cdot 6H_2O$, which was used as source of the catalytic active phase, following the same procedure as that used for the dopant agents. The Ni loading percentage was calculated considering the mass of the calcined doped support. The nomenclature employed for the produced catalysts is the following: BCCe*X*Ni*Y* or BCN*X*Ni*Y*, where *X* is the loading (wt.%) of ceria (Ce) or urea (N) and *Y* corresponds to the loading of nickel (Ni). Table S1 (in Supplementary Materials) summarizes all the produced materials and their nomenclatures.

2.2. Catalytic Experiments

Methanation tests were carried out in a tubular fixed-bed reactor (made of alloy UNS N10276), where around 1 g of catalyst was placed. The reactor was then filled with an inert material (Kaowool™ fiber) to avoid reactions outside of the catalytic bed. A K-type thermocouple was placed in the center of the catalytic bed to monitor the temperature evolution during the tests. Before each catalytic test, the bed was exposed to a reducing atmosphere (N_2/H_2, 90/10 vol.%) at 550 °C for 2.5 h to ensure the complete reduction of the nickel oxide. Once the preliminary reduction step was concluded, the reactor was cooled down to 300 °C under inert atmosphere and pressurized to the desired pressure value. Then, a mixture of $N_2/H_2/CO_2$ (50/40/10 vol.%) was fed to the reactor. Starting from 300 °C, the bed temperature was increased in steps of 50 °C and maintained constant for the time needed to obtain an almost constant product concentration. The composition of the outlet gaseous stream (CO, CO_2, CH_4, H_2, and light hydrocarbons such as C_2H_4, C_2H_6, and C_2H_2) was measured, using N_2 as internal standard, by means of a dual-channel micro-gas chromatograph (μ-GC 490 from Agilent, USA). A schematic representation of the experimental system is shown in Figure S1.

The catalytic activity of the tested samples was evaluated in terms of CO_2 conversion (X_{CO2}) and selectivity toward CO and CH_4 (S_{CO}, S_{CH4}), as defined in Equations (2)–(4). In these equations, F_i is the molar flow rate of the "*i*" species. The thermodynamic equilibrium values of X_{CO2}, S_{CO}, and S_{CH4} were calculated using the process simulation software Aspen Plus v_{10} (Gibbs free energy model).

$$X_{CO2} = (F_{CO2,\,in} - F_{CO2,\,out})\, F_{CO2,\,in}{}^{-1} \cdot 100 \quad (2)$$

$$S_{CH4} = F_{CH4,\,out}\, (F_{CO,\,out} + F_{CH4,\,out} + F_{C2H2,\,out} + F_{C2H6,\,out} + F_{C2H4,\,out})^{-1} \cdot 100 \quad (3)$$

$$S_{CO} = F_{CO,\,out}\, (F_{CO,\,out} + F_{CH4,\,out} + F_{C2H2,\,out} + F_{C2H6,\,out} + F_{C2H4,\,out})^{-1} \cdot 100 \quad (4)$$

2.3. Characterization of Carbon Materials

The textural characterization of the activated biochar (BC) and produced catalysts was performed from the N_2 adsorption/desorption isotherms at −196 °C, which were obtained using an ASAP 2020 automatic adsorption analyzer (Micromeritics, USA). Approximately 120 mg of sample was degassed under vacuum at 150 °C. The Langmuir model was adopted to evaluate the specific surface area (S_L). The total pore volume (V_{tot}) was calculated from the amount of N_2 adsorbed at high relative pressure (0.99). The specific volumes of micropores (V_{mic}), as well as the micro and mesopore surface area (S_{tmicro} and S_{tmeso}), were calculated using the *t*-plot method, whereas a non-local density functional theory (NLDFT) model assuming slit-pore geometry was used to evaluate the pore size distribution, from which the mesopore volume (V_{meso}) was estimated by subtracting the cumulative volume of micropores ($d_p < 2$ nm) from the total volume ($d_p < 50$ nm). The software MicroActive from Micromeritics was used for all the above-mentioned calculations.

The activated biochar (BC) was also characterized in terms of proximate analysis (in quadruplicate according to ASTM standards), ultimate analysis (using an analyzer

CHN628 from Leco Corporation, USA), and inorganic species (using an ADVANT'XP+XRF spectrometer from Thermo ARL, Switzerland).

The morphology features of both fresh and spent selected catalysts were observed by transmission electron microscopy (TEM) using a Tecnai F_{20} microscope (FEI, USA). Samples were previously sonicated for 5 min in an aqueous solution of ethanol. Furthermore, and in order to obtain information about the functional groups available in the surface, X-ray photoelectron spectroscopy (XPS) analyses were carried out using an XPS Spectrometer AXIS Supra (Kratos, UK) equipped with a mono Al Kα X-Ray source (120 W, 8 mA, 15 kV).

Temperature-programmed reduction (TPR) experiments were also conducted to evaluate the reducibility properties of the prepared catalysts. For these experiments, 0.5 g of each sample was loaded into the reactor used for the methanation tests and heated under a reducing stream (5% H_2 in Ar, at a flow rate of 0.5 NL min^{-1}) at a heating rate of 15 °C min^{-1} from 50 to 600 °C. The outlet hydrogen concentration was monitored online by means of a Hiden QGA analytical mass spectrometer.

3. Results

3.1. Effect of Ceria Loading

In the first stage, research was aimed at assessing the effect of the addition of ceria at different loadings (i.e., 10, 30, and 50 wt.%) on the performance of a Ni-based catalyst supported on the activated biochar. Nickel percentage in the catalyst formulation was kept constant at 40 wt.%, which was a commonly value reported in earlier studies [31,32]. As a preliminary step, the catalytic performance of the wheat straw activated biochar (BC) and the Ni-based catalyst (BCNi40) was tested. The obtained outcomes showed no catalytic activity in the case of BC, confirming that the carbonaceous support was completely inert under reaction conditions (data are not shown here). In the case of BCNi40, a maximum CO_2 conversion of 11% was reached at $_{1\cdot0}$ MPa and 500 °C (i.e., relative severe conditions) with almost null selectivity to CH_4 (see Figure S2).

Figure 1 summarizes the results obtained from catalytic tests conducted at a specific gas volumetric flow rate of 15 NL g^{-1} h^{-1}, at three absolute pressure values (0.35, 0.60, and 1.0 MPa), and temperatures in the range of 300–500 °C. As shown in Figure 1a, at 1.0 MPa the BCCe10Ni40 catalyst started to be active at 400 °C. However, and despite the increase in CO_2 conversion with the increase in temperature (with a maximum value of 40% at 500 °C), the observed high selectivity toward CO seems to confirm the dominant role of the reverse water gas shift (rWGS) reaction. Furthermore, as shown in Figure 1b,c, the BCCe10Ni40 catalyst was completely inactive at lower operating pressures.

The catalysts with higher amounts of ceria (30 and 50 wt.%) started to be active at 350 °C. In this case, the rWGS reaction was also the dominant reaction at relatively low temperatures, at which the CH_4 selectivity was very low (especially at 0.60 and 0.35 MPa). At 1.0 MPa, both the CO_2 conversion and selectivity toward CH_4 markedly increased with temperature in the range of 350–450 °C. At higher temperatures, a quasi-plateau was achieved for both variables.

In summary, we can conclude that, among the three tested catalysts, the BCCe30Ni40 showed the best catalytic activity for CO_2 methanation. In fact, at 1.0 MPa and 400 °C it was possible to reach 60% CO_2 conversion along with a selectivity toward methane of 90%. Therefore, it seems evident that ceria had a positive effect on the catalytic process, probably as a consequence of the introduced oxygen vacancies, which have a certain affinity for oxygen atoms present in CO_2 [33]. Furthermore, the introduction of CeO_2 leads to the formation of basic sites, which are essential for CH_4 production due to the enhancement of CO_2 adsorption [15]. Another positive effect of ceria is its ability to stabilize and better disperse the nickel species, leading to a stronger interaction between the catalytic active phase and its support [34]. However, excessive loadings of ceria (i.e., 50 wt.%) could result in a massive encapsulation of the support due to the formation of a ceria shell, which can lead to a significant loss in specific surface area and poorer dispersion of nickel species [16]. By contrast, low ceria loadings (i.e., 10 wt.%) could not be sufficient to ensure good extents

of CO_2 conversions toward methane, as proven by the high selectivity toward CO observed for both BCCe10Ni40 and BCNi40 catalysts.

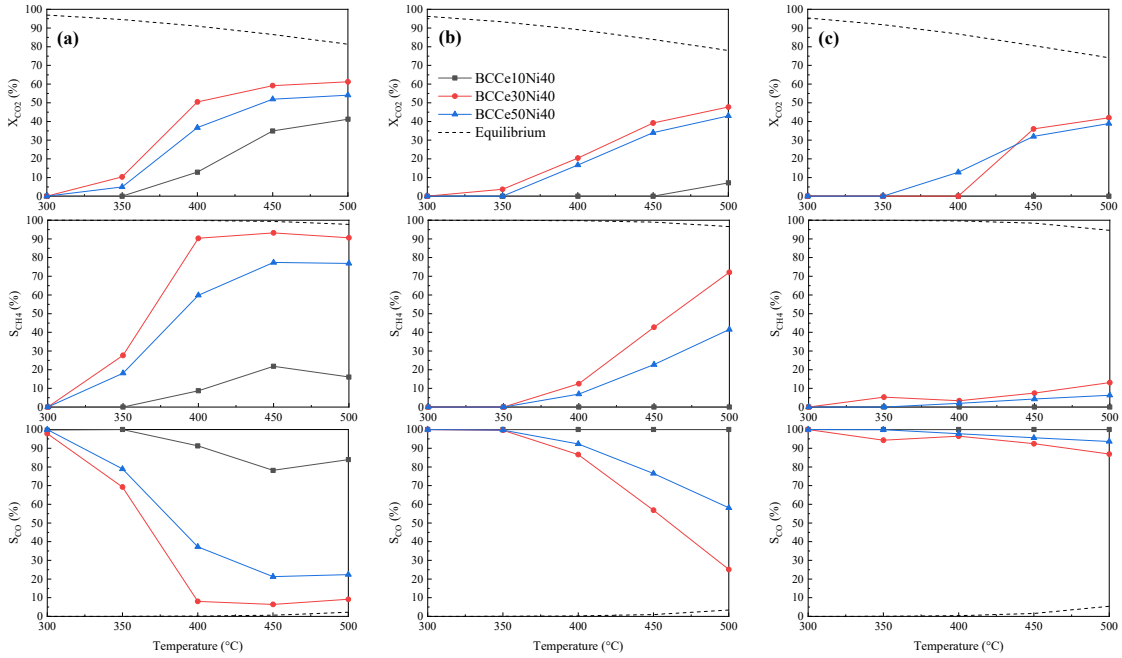

Figure 1. Results obtained using BCCeXNi40 at different ceria loadings during CO_2 methanation experiments, carried out at 15 NL g^{-1} h^{-1}, in the temperature range of 300–500 °C and at (**a**) 1.0 MPa, (**b**) 0.60 MPa, and (**c**) 0.35 MPa.

3.2. Effect of Nickel Loading

Once the optimal ceria loading was identified, Ni-CeO_2/BC catalysts with different Ni loadings (i.e., 10, 20, 30, and 40 wt.%) were tested under the same operating conditions used in the previous section. Results from the catalytic tests are displayed in Figure 2.

The decrease in Ni loading from 40 to 30 wt.% did not show a marked variation in the catalytic activity. CO_2 conversion gradually increased with the increase in temperature, reaching its maximum value at 500 °C. At this temperature and 1.0 MPa, the outlet stream was mainly composed of methane with a selectivity close to that at equilibrium. Interestingly, a further decrease in Ni loading (i.e., 10 and 20 wt.%) significantly enhanced the catalytic performance, especially at relatively lower temperatures. In fact, a selectivity toward CH_4 of almost 100% was observed for the BCCe30Ni20 catalyst at 350 °C and 1.0 MPa. This finding could be related to the fact that a high metal content could lead to particle agglomeration [35]. To further explore the effect of Ni loading, an additional catalytic test was carried out using the BCNi20 catalyst (without ceria doping) at 1.0 MPa. From Figure S2 (in which the catalytic performance of both BCNi20 and BCNi40 catalysts is shown), it can be deduced that an excessive Ni loading could lead to a critical decline in the catalytic activity due to the poorer dispersion of Ni within the carbon matrix. Furthermore, the synergistic role of ceria should also be highlighted, which significantly improved the catalytic performance of the BCNi20 catalyst (see Figure 2a and Figure S2 for comparative purposes).

On the other hand, a decrease in the absolute pressure resulted in an expected decrease in the catalytic activity (see Figure 2b,c). At lower pressures, CO_2 started to be reactive at higher temperatures. It was observed that the performance of the four tested catalysts showed a similar dependence on temperature, reaching the highest CO_2 conversion of ≈55% and ≈40% at 0.60 and 0.35 MPa, respectively. However, the selectivity toward CH_4 was strongly dependent on the Ni loading of the catalyst. In this sense, and in line with the remarks made above, the BCCe30Ni20 catalysts clearly exhibited the best catalytic

performance. The best Ni loading of 20 wt.% is in agreement with the results reported in previous studies for Ni-based catalysts supported on different materials [6,15].

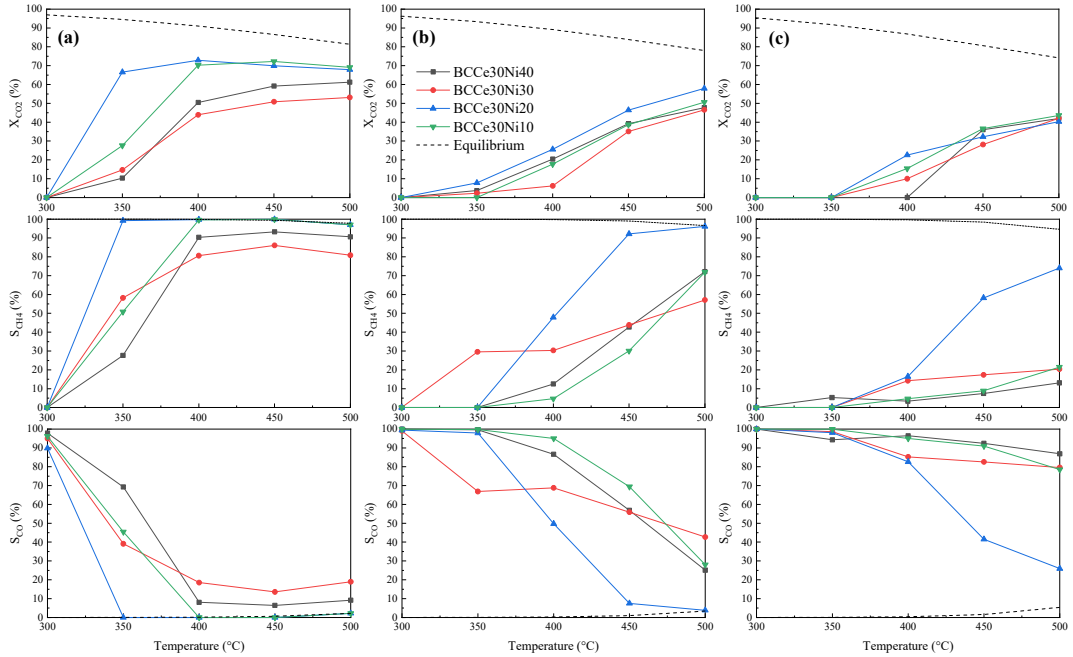

Figure 2. Results obtained during the study about the influence of Ni loadings on BCCe30 catalysts employed in CO_2 methanation experiments, which were carried out at 15 NL g^{-1} h^{-1}, in the temperature range of 300–500 °C and at (**a**) 1.0 MPa, (**b**) 0.60 MPa, and (**c**) 0.35 MPa.

3.3. Influence of Gas Space Velocity

Since CO_2 methanation is a highly exothermic process, a relatively high gas hourly space velocity (GHSV), usually greater than 10,000 h^{-1}, is required in order to avoid large temperature rises, which can affect both conversion and selectivity and also lead to a fast deactivation of the catalyst through metal phase sintering and/or encapsulation of active sites [20]. To explore the effect of GHSV, three different sets of experiments were carried out using the best catalyst (BCCe30Ni20) at the following gas volumetric flow rates: 15, 30, and 60 NL g^{-1} h^{-1}; which corresponded to 6600, 13,200, and 26,400 h^{-1}, respectively (apparent density of the catalyst = 440 kg m^{-3}). Results obtained from these experiments are summarized in Figure 3.

From the results obtained at 1.0 MPa (see Figure 3a), it was evident that the maximum carbon dioxide conversion was attained at 6600 h^{-1}, as expected. At this pressure and at temperatures higher than 400 °C, the catalytic performances, in terms of conversion and selectivity toward CH_4, at 15 and 30 NL g^{-1} h^{-1} were quite similar. The main difference lay in the catalyst activity at low temperatures (<400 °C), at which the lowest space velocity resulted in the highest CO_2 conversion. However, at lower operating pressures (see Figure 3b,c), an increase in GHSV dramatically affected the distribution of the products, leading to a marked increase in the selectivity toward CO at the expense of that toward methane.

Despite the fact that the CO_2 methanation reaction over Ni-based catalysts has been extensively investigated, there still are controversial views on the reaction mechanism. Two possible reaction pathways have been proposed so far: the formate route and the CO route. The first route involves the direct activation of the adsorbed CO_2 and subsequent formation of carbonates, which react with the dissociated hydrogen to produce formate species and, finally, methane [36]. The second possible mechanism firstly implies the conversion of CO_2 via rWGS to produce CO, which remains adsorbed on the active sites and is gradually hydrogenated to CH_4 [37]. The occurrence of one or another mechanism

could strictly be related to the properties of the catalyst support [33]. Ye et al. [38] studied the CO_2 methanation reaction mechanism over a Ni/CeO_2 catalyst and concluded that CO_2 was firstly adsorbed on the catalyst and then transformed into carbonate, bicarbonate, formate, and, finally, methane. However, and in light of the outcomes shown in Figure 3 (especially in terms of selectivity toward CO and CH_4), one can hypothesize that methane was produced through the CO route (rWGS and subsequent CO hydrogenation). The observed higher yields of CO at higher GHSV values could be explained by the fact that the gas residence time was not long enough to achieve complete hydrogenation of CO.

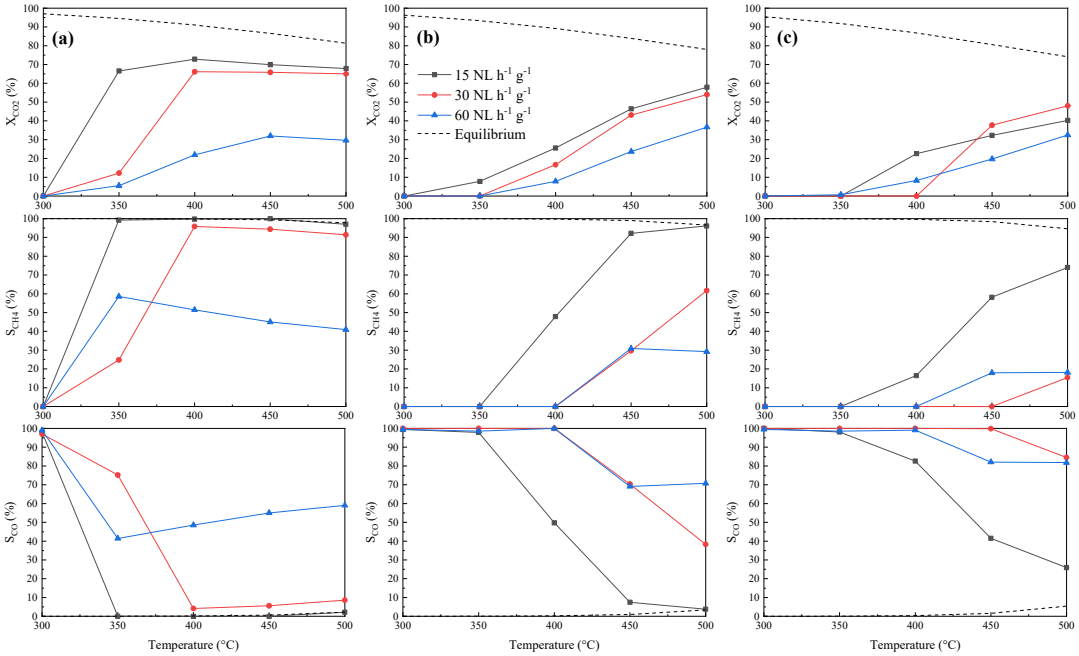

Figure 3. Study of the influence of gas space velocity on the catalytic performance of the BCCe30Ni20 catalyst. CO_2 methanation tests were conducted at 15, 30, and 60 NL g^{-1} h^{-1} (GHSV values of 6600, 13,200, and 26,400 h^{-1}, respectively), in the temperature range of 300–500 °C and at (**a**) 1.0 MPa, (**b**) 0.60 MPa, and (**c**) 0.35 MPa.

Since the catalytic performance of the BCCe30Ni20 catalyst at 1.0 MPa and temperatures starting from 400 °C was similar regardless of the gas space velocity tested (6600 or 13,200 h^{-1}), a specific gas volumetric flow rate of 30 NL g^{-1} h^{-1}, instead of 15 NL g^{-1} h^{-1}, is preferred from a practical point of view (13,200 h^{-1} is above the recommended threshold of 10,000 h^{-1}). Under this set of operating conditions, the BCCe30Ni20 catalyst exhibited a reasonably good activity, leading to conversion and selectivity values within the range reported in previous studies (see Table 1). The relatively low value of X_{CO2} observed for the catalyst developed in the present study could be related to the relatively high GHSV value used herein.

Table 1. CO_2 conversion and CH_4 selectivity values reported in some previous studies for catalytic CO_2 methanation.

Catalyst	Loading (wt.%)	Support	Pressure (MPa) and Temperature (°C)	Specific Gas Volumetric Flow Rate (NL g^{-1} h^{-1})	XCO_2 and SCH_4 (%)	Ref.
$Ni/\gamma\text{-}Al_2O_3$	12 (Ni)	Alumina	2, 210	-	80, 99.5	[39]
$35Ni_5Fe\_AX$	35(Ni)/5(Fe)	Xerogel	1, 220	9.6	63, 99.5	[40]
Fe/N-CNT	9.5 (Fe)	CNT	2.5, 350	50	25, 40	[41]
Ni/SiO_2	10 (Ni)	SiO_2	2, 310	20	77, 100	[42]
$Ni\text{-}15En/ZrO_2\text{-}1.5$	15 (Ni)	ZrO_2	0.5, 360	15	94, 97	[43]
Co/ZrO_2	2 (Co)	ZrO_2	3, 400	7.2	65, 99	[44]
Ni/Ce-ABC	15 (Ni)/15 (CeO_2)	Activated biochar	1, 400	6	87, 92	[28]
Ru/N-ABC	2 (Ru)	Activated biochar	1, 380	6	94, 100	[23]
BCCe30Ni20	20 (Ni)/30 (CeO_2)	Activated biochar	1, 400	30	65, 95	This work

3.4. N-Doping of the Carbonaceous Support

As an alternative to the use of CeO_2 as a dopant to improve the catalytic performance, the catalyst support (BC) was doped with urea. This kind of N-doping has been extensively assessed to improve the CO_2 uptake of activated carbon-based adsorbents [45]. Thermal decomposition of urea under an inert atmosphere leaves N atoms in the carbon lattice [46], which can stabilize Ni precursors in the support, enhancing the active phase dispersion (i.e., reducing the metallic particle size). Furthermore, N-doping could also increase the basicity of the support, which favors strong CO_2 adsorption [6]. To this end, the BCNi20 catalyst was doped with urea at three different loadings (i.e., 50, 67, and 75 wt.%), calcined at 500 °C under N_2, and then tested for CO_2 methanation at 1.0 MPa and 30 NL g^{-1} h^{-1}.

The results obtained at this stage are graphically summarized in Figure 4. As it can be deduced from the figure, the catalytic performance was progressively improved by increasing the loading of urea. By comparing the performances of the N-doped catalysts with that of the BCNi20 material, the beneficial effect of the urea addition was evident. Specifically, the higher the urea loading, the better the CO_2 conversion and methane selectivity. Even though the reactant conversions followed the same trend with the increase in temperature for all the tested samples, the production of methane became significant using a support:urea loading ratio greater than 1:0.5. The best results were obtained for the BCN75Ni20 catalyst at 500 °C, at which both the CO_2 conversion and selectivity toward CH_4 were equal to 45%. However, the catalytic performance of the best N-doped catalyst was clearly lower than that measured for the best ceria-doped catalyst (BCCe30Ni20), suggesting that using urea as dopant instead of ceria is not a recommended practice.

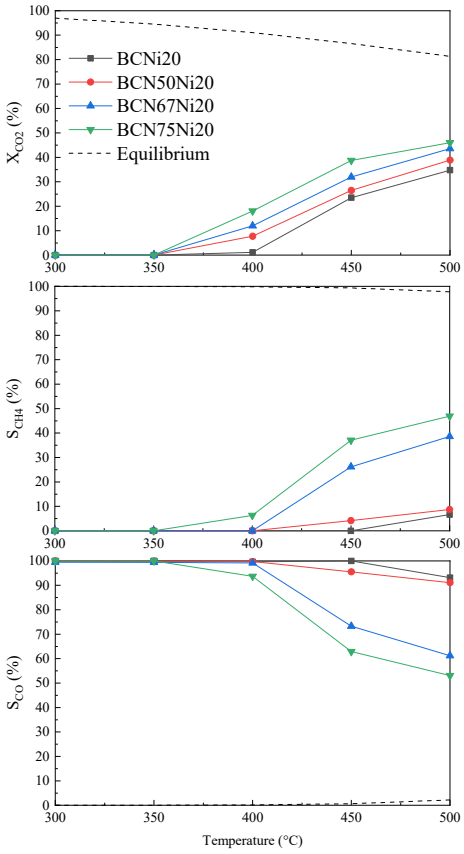

Figure 4. Catalytic performance of N-doped BCNi20 catalysts for CO_2 methanation experiments carried out at 30 NL g^{-1} h^{-1}, in the temperature range of 300–500 °C, and at 1.0 MPa.

3.5. Properties of Activated Biochar (BC) and Best-Performing Catalysts

In this section, the results from the characterization studies, which were mostly conducted for BC, BCCe30Ni20, and BCN75Ni20 materials, are presented.

For the wheat-straw-derived activated biochar used as support (BC), results from proximate, ultimate, and XRF analyses are reported in Table S2. As expected, the physical activation of pristine biochar resulted in a marked increase in the specific content of ashes. The composition of the inorganic matter revealed a high percentage of potassium, which can provide extra basic sites for CO_2 adsorption and activation.

Table S3 summarizes the textural properties of the three assessed materials. As can be seen, BC exhibited a highly microporous structure with a small volume of mesopores. For their part, both catalysts showed a remarkable decrease in specific surface area (compared to that of support) due to the impregnation and calcination steps. In addition, the observed decrease in the micropore volume was accompanied by an increase in the mesopore volume, probably caused by a certain collapse of the porous structure [47]. In this sense, a more hierarchical pore size distribution (with more mesopores) could be beneficial to enhance the diffusion of both reactants and products.

TPR analysis was performed on selected samples to evaluate the effect of CeO_2- and N-doping on the reduction of both the Ni-containing species and the support. From Figure S3, it can be seen that BC exhibited a reduction peak at relatively high temperatures (550 °C). Wang et al. [28] attributed this hydrogen consumption to the reduction of certain functional groups in the surface of carbonaceous support. Both the BCN75 and BCCe30 catalysts underwent reduction to some extent. For the BCCe30 material, the hydrogen consumption at 500 °C was mainly due to partial CeO_2 reduction at the surface, which was somewhat unexpected at such a low temperature [16]. This finding can probably be ascribed to the reductive properties of the carbon support [48]. On the other hand, hydrogen consumption in the range of 450–550 °C was observed for the BCN75 catalyst, although the mass spectrometer detected the presence of ammonia and the absence of water in the outlet stream. This result suggests that the calcination temperature was high enough to ensure the complete decomposition of the urea loaded; therefore, the surface of BC was mainly functionalized with C-N bonds. Some of these N-groups can undergo hydrogenation during TPR, leading to the observed release of NH_3.

Concerning the BCNi20 catalyst, the observed reduction of Ni-containing species at 400–550 °C is in agreement with previous studies [49]. As shown in Figure S3, two separated reduction peaks can be distinguished (α-peak at low temperature and β-peak at high temperature), which represents the portion of nickel bonded with the support through weak or strong interactions, respectively.

For both BCN75Ni20 and BCCe30Ni20 samples, Ni reduction can be observed at approximately 300 °C, which is an unusually low reduction temperature. This suggests that both ceria and urea doping strategies resulted in an improved reduction of NiO, which usually occurs at 500 °C for carbon-based supports [28]. It seems that Ni-Ce interactions increased the reducibility of NiO, generating more Ni sites that were accessible for the reactants to perform methanation [16]. Lower reduction temperatures usually indicate weaker metal–support interactions, which are not beneficial for the catalytic activity. However, for the specific case of the CO_2 methanation reaction, weak interactions are the factor main responsible for the reactant conversion [50,51]. Therefore, the high catalytic activity of the BCCe30Ni20 could be ascribed to the high reducibility of nickel oxide [17].

Figure 5 and Figure S4 show the TEM images for both BCCe30Ni20 and BCN75Ni20 catalysts before and after their employment in CO_2 methanation experiments at 30 NL g^{-1} h^{-1}, 400 °C, and 1.0 MPa. From Figure 5a,b (fresh BCCe30Ni20), it could be observed that a relatively good dispersion of Ni nanoparticles (NPs) was achieved for this catalyst. Nevertheless, the relatively high Ni loading resulted in some agglomerates, which are particularly visible in Figure 5b. The presence of metal NPs agglomerates was evident for the spent BCCe30Ni20 catalyst (see Figure 5c,d), which could be the main cause of catalyst deactivation [52]. Some earlier works ascribed the metal agglomeration to the formation of mobile species, which tend to migrate, causing Ni sintering and, consequently, catalyst deactivation [53]. Furthermore, Bartholomew et al. [54] stated that the water produced by methanation could accelerate the sintering process. On the other hand, Figure S4a,b shows that the N-doped BC support was

not as efficient as ceria in ensuring a good dispersion of Ni NPs. In this case, the spent sample also showed evident sintering phenomena (see Figure S4c,d). By comparing the TEM images of BCCe30Ni20 and BCN75Ni20 catalysts, it is possible to state that the improved nickel dispersion obtained after ceria introduction could be the main reason explaining the different catalytic outcomes observed for both materials.

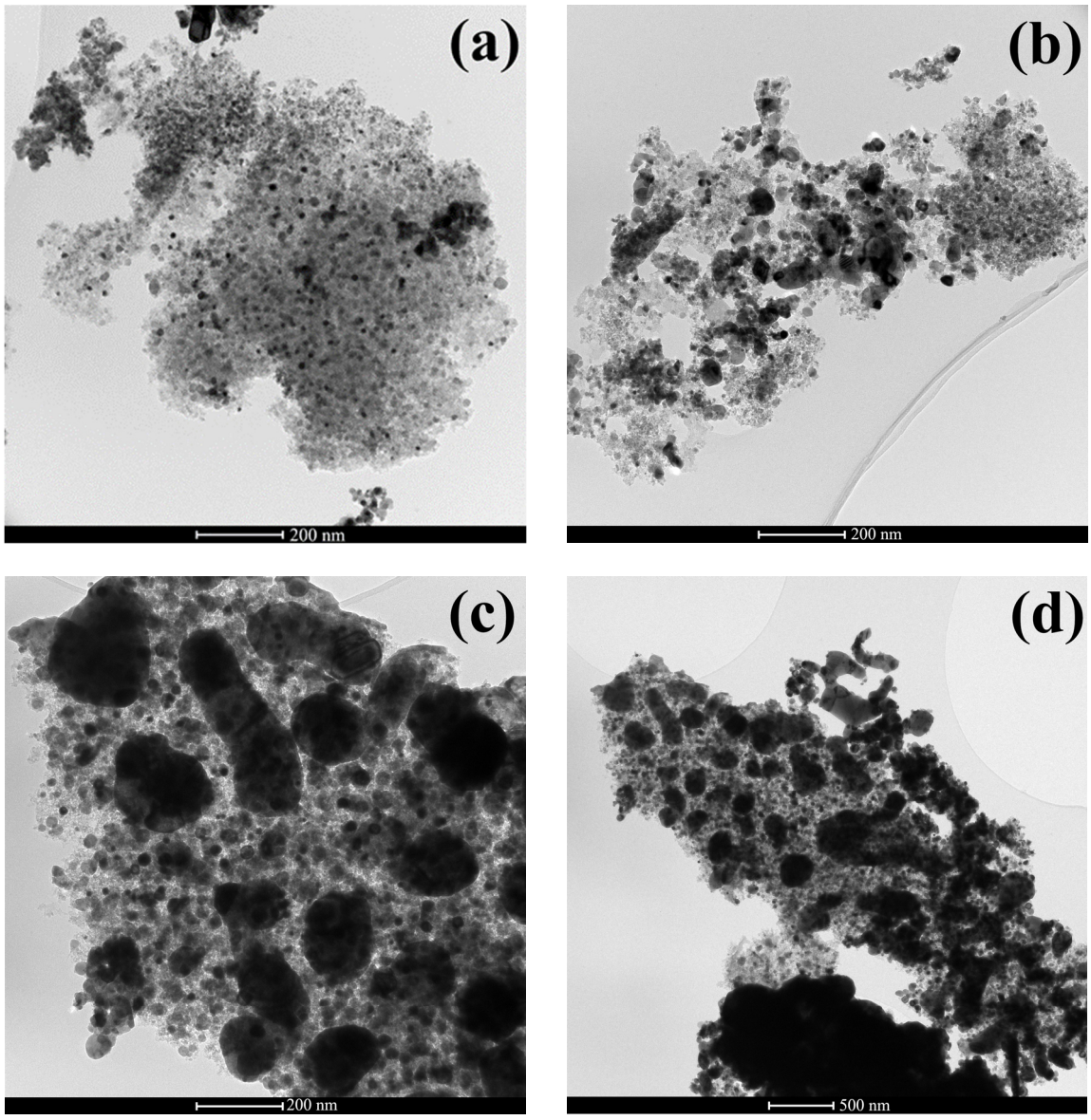

Figure 5. TEM images of BCCe30Ni20 catalyst: (**a**,**b**) fresh and (**c**,**d**) spent after CO_2 methanation at 30 NL g^{-1} h^{-1}, 400 °C and 1.0 MPa.

The full XPS spectra of the support (BC), as well as the fresh and spent BCN75Ni20 catalysts, are displayed in Figure S5. The elemental compositions calculated from the XPS analyses, which are listed in Table S4, indicate that N-doping was successfully implemented (higher atomic N:C ratios for N-doped materials). Furthermore, the huge decrease in Ni content in the spent catalyst could be ascribed to a certain encapsulation of the metal NPs inside carbon deposits, which resulted in a decrease in the metal fraction measured via XPS. The high-resolution spectra of the N1s binding energy region for the above-mentioned materials are shown in Figure S6. The spectra were deconvoluted into two peaks: pyridinic-N (398 eV) [23] and pyrrolic-N (400.8 eV) [55]. Figure S6 clearly shows that BC contained a certain number of N-containing functional groups, which originated

from the biomass precursor, as already confirmed by the ultimate analysis (see Table S2). Urea doping resulted in higher pyridinic-N content, with respect to the undoped support. As can deduced from Figure S6, the contents of both pyridinic- and pyrrolic-N remained almost constant after the catalytic test, suggesting the relative stability of these functional groups under the tested operating conditions.

4. Conclusions

Using wheat straw activated biochar loaded with 30 wt.% of ceria and 20 wt.% of nickel, it was possible to obtain a CO_2 conversion of 65% and a selectivity toward CH_4 of 95% at 1.0 MPa, 400 °C, and 13,200 h^{-1}. The rWGS-CO hydrogenation route was proposed as a reaction mechanism. Despite the fact that using urea as a dopant resulted in the introduction of nitrogenated functionalities in the surface of BC, the improvement of the catalytic activity of the resulting catalyst was modest in comparison to that attained when ceria was used as dopant.

Supplementary Materials: The following are available online at https://www.mdpi.com/article/10.3390/su13168939/s1, Table S1: Summary of all the catalysts synthesized and tested in this work; Table S2: Proximate, ultimate, and inorganic matter analysis; Table S3: Textural characterization; Table S4: Surface composition measured by XPS; Figure S1: Schematic overview of the experimental device; Figure S2: Results obtained during methanation experiments using the BCNi20 and BCNi40; Figure S3: Hydrogen uptake profiles from TPR for different materials; Figure S4: TEM images of BCN75Ni20; Figure S5: Full XPS spectra; Figure S6: XPS high-resolution spectra; Nomenclature.

Author Contributions: Conceptualization, C.D.S., J.J.M. and S.R.; methodology, C.D.S., G.G. and S.R.; validation, J.J.M., B.G. and V.P.; formal analysis, C.D.S.; data curation, C.D.S., S.R., J.J.M. and V.P.; writing—original draft preparation, C.D.S. and J.J.M.; writing—review and editing, G.G., S.R., J.J.M., B.G. and V.P.; supervision, J.J.M.; project administration, J.J.M.; funding acquisition, J.J.M. All authors have read and agreed to the published version of the manuscript.

Funding: This project received funding from the European Union's Horizon 2020 research and innovation program under the Marie Skłodowska-Curie grant agreement No 721991. The authors also acknowledge the funding from the Aragón Government (Ref. T22_20R), co-funded by FEDER 2014–2020 "Construyendo Europa desde Aragón".

Acknowledgments: The authors gratefully thank José Antonio Manso, Olga Marín, and Miguel González for their help in the preparation and characterization of the samples. Authors would like to acknowledge the use of Servicio General de Apoyo a la Investigación-SAI, Universidad de Zaragoza.

Conflicts of Interest: The authors declare no conflict of interest.

References

1. Butenschön, M.; Lovato, T.; Masina, S.; Caserini, S.; Grosso, M. Alkalinization Scenarios in the Mediterranean Sea for Efficient Removal of Atmospheric CO_2 and the Mitigation of Ocean Acidification. *Front. Clim.* **2021**, *3*, 1–11. [CrossRef]
2. de Souza Mendonça, A.K.; de Silva, S.A.; Pereira, L.Z.; Bornia, A.C.; de Andrade, D.F. An Overview of Environmental Policies for Mitigation and Adaptation to Climate Change and Application of Multilevel Regression Analysis to Investigate the CO_2 Emissions over the Years of 1970 to 2018 in All Brazilian States. *Sustainability* **2020**, *12*, 9175. [CrossRef]
3. Huang, W.-J.; Kao, K.-J.; Liu, L.-L.; Liao, C.-W.; Han, Y.-L. An Assessment of Direct Dissolved Inorganic Carbon Injection to the Coastal Region: A Model Result. *Sustainability* **2018**, *10*, 1174. [CrossRef]
4. Baena-Moreno, F.M.; Rodríguez-Galán, M.; Vega, F.; Alonso-Fariñas, B.; Vilches Arenas, L.F.; Navarrete, B. Carbon capture and utilization technologies: A literature review and recent advances. *Energy Sources Part A Recover. Util. Environ. Eff.* **2019**, *41*, 1403–1433. [CrossRef]
5. Thema, M.; Bauer, F.; Sterner, M. Power-to-Gas: Electrolysis and methanation status review. *Renew. Sustain. Energy Rev.* **2019**, *112*, 775–787. [CrossRef]
6. Gonçalves, L.P.L.; Sousa, J.P.S.; Soares, O.S.G.P.; Bondarchuk, O.; Lebedev, O.I.; Kolen'Ko, Y.V.; Pereira, M.F. The role of surface properties in CO_2 methanation over carbon-supported Ni catalysts and their promotion by Fe. *Catal. Sci. Technol.* **2020**, *10*, 7217–7225. [CrossRef]
7. Petersen, E.M.; Rao, R.G.; Vance, B.C.; Tessonnier, J.-P. SiO_2/SiC supports with tailored thermal conductivity to reveal the effect of surface temperature on Ru-catalyzed CO_2 methanation. *Appl. Catal. B Environ.* **2021**, *286*, 119904. [CrossRef]

8. Younas, M.; Sethupathi, S.; Kong, L.L.; Mohamed, A.R.; Muhammad, Y. CO_2 methanation over Ni and Rh based catalysts: Process optimization at moderate temperature. *Int. J. Energy Res.* **2018**, *42*, 3289–3302. [CrossRef]
9. Renda, S.; Ricca, A.; Palma, V. Study of the effect of noble metal promotion in Ni-based catalyst for the Sabatier reaction. *Int. J. Hydrog. Energy* **2021**, *46*, 12117–12127. [CrossRef]
10. Garbarino, G.; Kowalik, P.; Riani, P.; Antoniak-Jurak, K.; Pieta, P.; Lewalska-Graczyk, A.; Lisowski, W.; Nowakowski, R.; Busca, G.; Pieta, I.S. Improvement of Ni/Al_2O_3 Catalysts for Low-Temperature CO_2 Methanation by Vanadium and Calcium Oxide Addition. *Ind. Eng. Chem. Res.* **2021**, *60*, 6554–6564. [CrossRef]
11. Agnelli, M.; Swaan, H.; Marquez-Alvarez, C.; Martin, G.; Mirodatos, C. CO Hydrogenation on a Nickel Catalyst: II. A Mechanistic Study by Transient Kinetics and Infrared Spectroscopy. *J. Catal.* **1998**, *175*, 117–128. [CrossRef]
12. Zhang, Z.; Tian, Y.; Zhang, L.; Hu, S.; Xiang, J.; Wang, Y.; Xu, L.; Liu, Q.; Zhang, S.; Hu, X. Impacts of nickel loading on properties, catalytic behaviors of Ni/γ–Al_2O_3 catalysts and the reaction intermediates formed in methanation of CO. *Int. J. Hydrog. Energy* **2019**, *44*, 9291–9306. [CrossRef]
13. Wolf, M.; Wong, L.H.; Schüler, C.; Hinrichsen, O. CO_2 methanation on transition-metal-promoted Ni-Al catalysts: Sulfur poisoning and the role of CO_2 adsorption capacity for catalyst activity. *J. CO2 Util.* **2020**, *36*, 276–287. [CrossRef]
14. Li, W.; Nie, X.; Jiang, X.; Zhang, A.; Ding, F.; Liu, M.; Liu, Z.; Guo, X.; Song, C. ZrO_2 support imparts superior activity and stability of Co catalysts for CO_2 methanation. *Appl. Catal. B Environ.* **2018**, *220*, 397–408. [CrossRef]
15. Hu, F.; Tong, S.; Lu, K.; Chen, C.-M.; Su, F.-Y.; Zhou, J.; Lu, Z.-H.; Wang, X.; Feng, G.; Zhang, R. Reduced graphene oxide supported Ni-Ce catalysts for CO_2 methanation: The support and ceria promotion effects. *J. CO2 Util.* **2019**, *34*, 676–687. [CrossRef]
16. Alarcón, A.; Guilera, J.; Díaz-López, J.A.; Andreu, T. Optimization of nickel and ceria catalyst content for synthetic natural gas production through CO_2 methanation. *Fuel Process. Technol.* **2019**, *193*, 114–122. [CrossRef]
17. Cam, L.M.; Ha, N.T.T.; Van Khu, L.; Brown, T.C.; Ha, N.N. Carbon Dioxide Methanation Over Nickel Catalysts Supported on Activated Carbon at Low Temperature. *Aust. J. Chem.* **2019**, *72*, 969. [CrossRef]
18. Feng, Y.; Yang, W.; Chu, W. Effect of Ca modification on the catalytic performance of Ni/AC for CO_2 methanation. *Integr. Ferroelectr.* **2016**, *172*, 40–48. [CrossRef]
19. Wang, W.; Chu, W.; Wang, N.; Yang, W.; Jiang, C. Mesoporous nickel catalyst supported on multi-walled carbon nanotubes for carbon dioxide methanation. *Int. J. Hydrog. Energy* **2016**, *41*, 967–975. [CrossRef]
20. Wang, W.; Duong-Viet, C.; Ba, H.; Baaziz, W.; Tuci, G.; Caporali, S.; Nguyen-Dinh, L.; Ersen, O.; Giambastiani, G.; Pham-Huu, C. Nickel Nanoparticles Decorated Nitrogen-Doped Carbon Nanotubes (Ni/N-CNT); a Robust Catalyst for the Efficient and Selective CO_2 Methanation. *ACS Appl. Energy Mater.* **2018**, *2*, 1111–1120. [CrossRef]
21. Antoniak-Jurak, K.; Kowalik, P.; Konkol, M.; Próchniak, W.; Bicki, R.; Raróg-Pilecka, W.; Kuśtrowski, P.; Ryczkowski, J. Sulfur tolerant Co–Mo–K catalysts supported on carbon materials for sour gas shift process—Effect of support modification. *Fuel Process. Technol.* **2016**, *144*, 305–311. [CrossRef]
22. Antoniak-Jurak, K.; Kowalik, P.; Próchniak, W.; Raróg-Pilecka, W.; Kuśtrowski, P.; Ryczkowski, J. Sour gas shift process over sulfided Co–Mo–K catalysts supported on carbon material—Support characterization and catalytic activity of catalysts. *Fuel Process. Technol.* **2015**, *138*, 305–313. [CrossRef]
23. Wang, X.; Liu, Y.; Zhu, L.; Li, Y.; Wang, K.; Qiu, K.; Tippayawong, N.; Aggarangsi, P.; Reubroycharoen, P.; Wang, S. Biomass derived N-doped biochar as efficient catalyst supports for CO_2 methanation. *J. CO2 Util.* **2019**, *34*, 733–741. [CrossRef]
24. Ashok, J.; Pati, S.; Hongmanorom, P.; Tianxi, Z.; Junmei, C.; Kawi, S. A review of recent catalyst advances in CO_2 methanation processes. *Catal. Today* **2020**, *356*, 471–489. [CrossRef]
25. Manyà, J.J. Pyrolysis for Biochar Purposes: A Review to Establish Current Knowledge Gaps and Research Needs. *Environ. Sci. Technol.* **2012**, *46*, 7939–7954. [CrossRef] [PubMed]
26. Wang, S.; Wang, H.; Yin, Q.; Zhu, L.; Yin, S. Methanation of bio-syngas over a biochar supported catalyst. *New J. Chem.* **2014**, *38*, 4471–4477. [CrossRef]
27. Dufour, A.; Celzard, A.; Fierro, V.; Martin, E.; Broust, F.; Zoulalian, A. Catalytic decomposition of methane over a wood char concurrently activated by a pyrolysis gas. *Appl. Catal. A Gen.* **2008**, *346*, 164–173. [CrossRef]
28. Wang, X.; Yang, M.; Zhu, X.; Zhu, L.; Wang, S. Experimental study and life cycle assessment of CO_2 methanation over biochar supported catalysts. *Appl. Energy* **2020**, *280*, 115919. [CrossRef]
29. Greco, G.; Di Stasi, C.; Rego, F.; González, B.; Manyà, J.J. Effects of slow-pyrolysis conditions on the products yields and properties and on exergy efficiency: A comprehensive assessment for wheat straw. *Appl. Energy* **2020**, *279*, 115842. [CrossRef]
30. Di Stasi, C.; Greco, G.; Canevesi, R.L.S.; Izquierdo, M.T.; Fierro, V.; Celzard, A.; González, B.; Manyà, J.J. Influence of activation conditions on textural properties and performance of activated biochars for pyrolysis vapors upgrading. *Fuel* **2021**, *289*, 119759. [CrossRef]
31. Gnanakumar, E.S.; Chandran, N.; Kozhevnikov, I.V.; Grau-Atienza, A.; Ramos-Fernandez, E.V.; Sepulveda-Escribano, A.; Shiju, N.R. Highly efficient nickel-niobia composite catalysts for hydrogenation of CO_2 to methane. *Chem. Eng. Sci.* **2019**, *194*, 2–9. [CrossRef]
32. Hwang, S.; Lee, J.; Hong, U.G.; Gil Seo, J.; Jung, J.C.; Koh, D.J.; Lim, H.; Byun, C.; Song, I.K. Methane production from carbon monoxide and hydrogen over nickel–alumina xerogel catalyst: Effect of nickel content. *J. Ind. Eng. Chem.* **2011**, *17*, 154–157. [CrossRef]

33. Shen, L.; Xu, J.; Zhu, M.; Han, Y.-F. Essential Role of the Support for Nickel-Based CO_2 Methanation Catalysts. *ACS Catal.* **2020**, *10*, 14581–14591. [CrossRef]
34. Le, M.C.; Van, K.L.; Nguyen, T.H.T.; Nguyen, N.H. The Impact of Ce-Zr Addition on Nickel Dispersion and Catalytic Behavior for CO_2 Methanation of Ni/AC Catalyst at Low Temperature. *J. Chem.* **2017**, *2017*, 1–11. [CrossRef]
35. Gödde, J.; Merko, M.; Xia, W.; Muhler, M. Nickel nanoparticles supported on nitrogen–doped carbon nanotubes are a highly active, selective and stable CO_2 methanation catalyst. *J. Energy Chem.* **2021**, *54*, 323–331. [CrossRef]
36. Fatah, N.; Jalil, A.; Salleh, N.; Hamid, M.; Hassan, Z.; Nawawi, M.G.M. Elucidation of cobalt disturbance on Ni/Al_2O_3 in dissociating hydrogen towards improved CO_2 methanation and optimization by response surface methodology (RSM). *Int. J. Hydrog. Energy* **2020**, *45*, 18562–18573. [CrossRef]
37. Yan, B.; Zhao, B.; Kattel, S.; Wu, Q.; Yao, S.; Su, D.; Chen, J.G. Tuning CO_2 hydrogenation selectivity via metal-oxide interfacial sites. *J. Catal.* **2019**, *374*, 60–71. [CrossRef]
38. Ye, R.-P.; Li, Q.; Gong, W.; Wang, T.; Razink, J.J.; Lin, L.; Qin, Y.-Y.; Zhou, Z.; Adidharma, H.; Tang, J.; et al. High-performance of nanostructured Ni/CeO_2 catalyst on CO_2 methanation. *Appl. Catal. B Environ.* **2020**, *268*, 118474. [CrossRef]
39. Lim, J.Y.; McGregor, J.; Sederman, A.; Dennis, J. Kinetic studies of CO 2 methanation over a Ni/γ-Al_2O_3 catalyst using a batch reactor. *Chem. Eng. Sci.* **2016**, *141*, 28–45. [CrossRef]
40. Hwang, S.; Hong, U.G.; Lee, J.; Baik, J.H.; Koh, D.J.; Lim, H.; Song, I.K. Methanation of Carbon Dioxide Over Mesoporous Nickel–M–Alumina (M = Fe, Zr, Ni, Y, and Mg) Xerogel Catalysts: Effect of Second Metal. *Catal. Lett.* **2012**, *142*, 860–868. [CrossRef]
41. Chew, L.M.; Kangvansura, P.; Ruland, H.; Schulte, H.J.; Somsen, C.; Xia, W.; Eggeler, G.; Worayingyong, A.; Muhler, M. Effect of nitrogen doping on the reducibility, activity and selectivity of carbon nanotube-supported iron catalysts applied in CO_2 hydrogenation. *Appl. Catal. A Gen.* **2014**, *482*, 163–170. [CrossRef]
42. Ye, R.-P.; Liao, L.; Reina, T.R.; Liu, J.; Chevella, D.; Jin, Y.; Fan, M.; Liu, J. Engineering Ni/SiO_2 catalysts for enhanced CO_2 methanation. *Fuel* **2021**, *285*, 119151. [CrossRef]
43. Quan, Y.; Zhang, N.; Zhang, Z.; Han, Y.; Zhao, J.; Ren, J. Enhanced performance of Ni catalysts supported on ZrO_2 nanosheets for CO_2 methanation: Effects of support morphology and chelating ligands. *Int. J. Hydrog. Energy* **2021**, *46*, 14395–14406. [CrossRef]
44. Li, W.; Liu, Y.; Mu, M.; Ding, F.; Liu, Z.; Guo, X.; Song, C. Organic acid-assisted preparation of highly dispersed Co/ZrO2 catalysts with superior activity for CO_2 methanation. *Appl. Catal. B Environ.* **2019**, *254*, 531–540. [CrossRef]
45. Sivadas, D.L.; Vijayan, S.; Rajeev, R.; Ninan, K.; Prabhakaran, K. Nitrogen-enriched microporous carbon derived from sucrose and urea with superior CO_2 capture performance. *Carbon* **2016**, *109*, 7–18. [CrossRef]
46. Lin, Z.; Waller, G.; Liu, Y.; Liu, M.; Wong, C.-P. Facile Synthesis of Nitrogen-Doped Graphene via Pyrolysis of Graphene Oxide and Urea, and its Electrocatalytic Activity toward the Oxygen-Reduction Reaction. *Adv. Energy Mater.* **2012**, *2*, 884–888. [CrossRef]
47. Kumar, A.; Sinha, A. Hydrogen production from acetic acid steam reforming over nickel-based catalyst synthesized via MOF process. *Int. J. Hydrog. Energy* **2020**, *45*, 24397–24411. [CrossRef]
48. Quan, C.; Wang, H.; Gao, N. Development of activated biochar supported Ni catalyst for enhancing toluene steam reforming. *Int. J. Energy Res.* **2020**, *44*, 5749–5764. [CrossRef]
49. Chen, J.; Wang, M.; Wang, S.; Li, X. Hydrogen production via steam reforming of acetic acid over biochar-supported nickel catalysts. *Int. J. Hydrog. Energy* **2018**, *43*, 18160–18168. [CrossRef]
50. Li, M.; Amari, H.; van Veen, A.C. Metal-oxide interaction enhanced CO_2 activation in methanation over ceria supported nickel nanocrystallites. *Appl. Catal. B: Environ.* **2018**, *239*, 27–35. [CrossRef]
51. Zhu, M.; Tian, P.; Kurtz, R.; Lunkenbein, T.; Xu, J.; Schlögl, R.; Wachs, I.E.; Han, Y. Strong Metal–Support Interactions between Copper and Iron Oxide during the High-Temperature Water-Gas Shift Reaction. *Angew. Chem. Int. Ed.* **2019**, *58*, 9083–9087. [CrossRef] [PubMed]
52. Coll, R.; Salvadó, J.; Farriol, X.; Montané, D. Steam reforming model compounds of biomass gasification tars: Conversion at different operating conditions and tendency towards coke formation. *Fuel Process. Technol.* **2001**, *74*, 19–31. [CrossRef]
53. Miao, B.; Ma, S.S.K.; Wang, X.; Su, H.; Chan, S.H. Catalysis mechanisms of CO_2 and CO methanation. *Catal. Sci. Technol.* **2016**, *6*, 4048–4058. [CrossRef]
54. Bartholomew, C. Sintering of alumina-supported nickel and nickel bimetallic methanation catalysts in H_2/H_2O atmospheres. *J. Catal.* **1983**, *79*, 34–46. [CrossRef]
55. Li, K.; Chen, W.; Yang, H.; Chen, Y.; Xia, S.; Xia, M.; Tu, X.; Chen, H. Mechanism of biomass activation and ammonia modification for nitrogen-doped porous carbon materials. *Bioresour. Technol.* **2019**, *280*, 260–268. [CrossRef]